Role of aperiodic order for fluxon dynamics in Josephson junction arrays

Erik Lennholm* and Michael Hörnquist†
Department of Physics and Measurement Technology, Linköping University, S-581 83 Linköping, Sweden
(Received 26 August 1998)

We perform numerical simulations of a kink-shaped soliton, a fluxon, propagating in arrays of Josephson junctions ordered according to the period-doubling sequence, the Fibonacci sequence, the paper-folding sequence, the Rudin-Shapiro sequence, and the Thue-Morse sequence. The equation of motion is the discrete sine-Gordon equation with additional terms describing dissipation and an injected bias current. With the use of an effective potential we explain the behavior of the fluxon when it gets pinned in different arrays. The potential also gives a qualitative understanding of the deviation of the velocity of a propagating fluxon compared with an earlier obtained formula. It turns out that the self-similarity of the underlying sequences is important for the detailed dynamics, but not for the speed of a propagating fluxon. Finally, we show how this effective potential can be used to arrange an array to have some desired properties. [S1063-651X(99)05501-4]

PACS number(s): 05.45.Gg, 85.25.Cp, 45.05.+x, 02.10.Gd

I. INTRODUCTION

The discrete sine-Gordon equation has been extensively studied from different viewpoints during recent years, see, e.g., Ref. [1] and references therein. It is an equation suitable to describe several different physical phenomena, among which we can mention DNA promoter dynamics [2], the Frenkel-Kontorova model [3], and Josephson junctions [4].

The study of aperiodically ordered structures was for a long time of interest only for mathematicians. However, the discovery of incommensurate crystals in the 1960s [5] and of quasicrystals in 1984 [6] has inspired a large amount of both theoretical and experimental work among physicists concerning different systems with order between periodic and random. These systems not only comprise what is found in nature, but also man-made materials such as superlattices, the first aperiodic one built already in 1985 [7]. Recently, there have also been some suggestions of other man-made systems with a possibility to possess aperiodic order. Examples are quantum dots [8] and Josephson junction arrays [9]. The latter has today reached a stage where the technology is even commercially available, see, e.g., Ref. [10].

In this paper, we focus upon one-dimensional arrays of Josephson junctions ordered according to some different aperiodic sequences in order to understand such behavior as soliton propagation and soliton pinning as functions of the underlying sequence. The soliton in question is a single kink soliton known as a fluxon. To do this, we use an effective potential previously developed in Ref. [2] for treating problems of this kind.

Properly rescaled to dimensionless units, the motion of the soliton (the phase) in a Josephson junction array is described by

$$\frac{\partial^2\phi_n}{\partial t^2}-\frac{1}{a^2}(\phi_{n+1}+\phi_{n-1}-2\phi_n)=-q_n\sin\phi_n-\alpha\frac{\partial\phi_n}{\partial t}-F. \tag{1}$$

Compared with the ''normal'' discrete sine-Gordon equation (a being the discreteness parameter), we have inserted a term $\alpha\partial\phi_n/\partial t$ to model the dissipation due to normal electrons tunneling across the barriers, a term F to describe a bias current which is injected in every junction, and the material parameters q_n.

The sequences according to which we will order our junctions are the period-doubling sequence, the Fibonacci sequence, the Thue-Morse sequence, the paper-folding sequence, and finally the Rudin-Shapiro sequence. These sequences are now well known and their construction can be found in numerous papers. Nevertheless, we summarize in Table I how they can be generated by the use of substitution rules. The first 16 elements of each sequence are also shown. More detailed descriptions of these sequences, except the paper-folding sequence, can be found in, e.g., Ref. [11]. The remaining one can be found in Ref. [12]. As comparisons, we will also include some results from arrays ordered periodically and randomly. The entity from Eq. (1) which will be varied aperiodically is the material parameter q_n, to which we will assign two different, positive values q_A and q_B, such that $q_n=q_A(q_B)$ if the nth element of the sequence is an $A(B)$.

In the next section (II), the model and the parameter values used for the numerical simulations are presented. In Sec. III we will introduce the effective potential used to describe our numerical simulations. The results are described in Sec. IV and finally in Sec. V we make a summary.

II. MODEL

The discrete sine-Gordon equation is nonintegrable, and we study it numerically. We have chosen a fourth-order Runge-Kutta method with a time-step size of either 10^{-3} or 10^{-4}. The smaller step size is mainly used in simulations which cover times $t>50$, because otherwise we cannot guarantee the validity of the solutions. We have also performed simulations for $t<50$ with different step sizes and found that the results are equivalent. This indicates that the numerical algorithm used for the integration is acceptable.

As initial conditions we take $\phi_n(n_0,t=0)$

*Electronic address: erile@ifm.liu.se
†Electronic address: micho@ifm.liu.se

TABLE I. Substitution rules and the beginning of the sequences we use in this paper.

Sequence	Substitution rule	Start of the sequence
Fibonacci	$A\rightarrow AB,\ B\rightarrow A$	$ABAABABAABAABABA\cdots$
Thue-Morse	$A\rightarrow AB,\ B\rightarrow BA$	$ABBABAABBAABABBA\cdots$
Period-doubling	$A\rightarrow AB,\ B\rightarrow AA$	$ABAAABABABAAABAA\cdots$
Paper-folding	$a\rightarrow ab,\ b\rightarrow cb,\ c\rightarrow ad,\ d\rightarrow cd$	
	$a\rightarrow A,\ b\rightarrow A,\ c\rightarrow B,\ d\rightarrow B$	$AABAABBAAABBABBA\cdots$
Rudin-Shapiro	$a\rightarrow ab,\ b\rightarrow ac,\ c\rightarrow db,\ d\rightarrow dc$	
	$a\rightarrow A,\ b\rightarrow A,\ c\rightarrow B,\ d\rightarrow B$	$AAABAABAAAABBBAB\cdots$

$=4\arctan\{\exp[a(n-n_0)/(1-u^2)^{1/2}]\}$ and $\dot{\phi}_n(n_0,t=0)=[-2u/(1-u^2)^{1/2}]\mathrm{sech}[a(n-n_0)/(1-u^2)^{1/2}]$, which are nothing but the discrete values for $1\leqslant n\leqslant N$ of the approximative single fluxon solution to the perturbed continuous sine-Gordon equation ($x=na$)

$$\frac{\partial^2\phi}{\partial t^2}-\frac{\partial^2\phi}{\partial x^2}=-\sin\phi-\alpha\frac{\partial\phi}{\partial t}-F. \tag{2}$$

Here n_0 is the starting site for the fluxon, and

$$u=\left[1+\left(\frac{4\alpha}{\pi F}\right)^2\right]^{-1/2} \tag{3}$$

is the fluxon velocity in the limit of balance between the injected power and the dissipation for a Josephson junction transmission line [13]. We use fixed boundary conditions according to

$$\phi_n=\begin{cases}0, & n=0\\ 2\pi, & n=N+1,\end{cases}\quad \dot{\phi}_n=\begin{cases}0, & n=0\\ 0, & n=N+1.\end{cases} \tag{4}$$

Unless otherwise specified, we have used the following values for the parameters in the model.

(i) The discreteness parameter $a=0.1$. This choice leads to a discrete array but still close to the continuous limit.

(ii) The dissipative constant $\alpha=0.1$. When the fluxon propagates with constant velocity, the power injected through the bias current (F) is balanced by the power dissipated by the α term. This means that there is a close connection between α and F, where α fixes the scale for F.

(iii) The material parameter $q_A=1$ without loss of generality, and q_B ranges from 1 to 20.

(iv) The number of junctions in the array N varies between 256 and 4096. The starting site n_0 is somewhere in the middle of the array so that the fluxon can propagate without interference from the boundaries.

While numerically integrating Eq. 1, we will also keep track of the position of the fluxon center, i.e., the position along the x axis where $\phi=\pi$. Since this will seldom be at a position of an actual junction, a linear interpolation is performed between the two sites which enclose the fluxon center.

III. AN EFFECTIVE POTENTIAL

In order to describe the motion of the soliton in arrays ordered according to the different sequences, we will use an approach originally developed by Salerno and Kivshar [2]. If we neglect the dissipative effect, the Hamiltonian leading to Eq. 1 consists only of conservative energy terms so the Hamiltonian is the same as the energy E for the system,

$$E=\sum_{n=1}^{N}\left\{\frac{1}{2}\dot{\phi}_n^2+\frac{1}{2a^2}(\phi_{n+1}-\phi_n)^2+q_n(1-\cos\phi_n)+F\phi_n\right\}. \tag{5}$$

The energy in this case is conserved. The fact that we have overlooked the dissipation term in the approximation implies that we have to restrict the analysis to the beginning of the soliton motion where the effects of the dissipation are small. It is well known that the continuous unperturbed (no dissipation and bias terms) sine-Gordon equation has different analytical soliton solutions, e.g., single fluxons, multikink fluxons, and breathers [13]. Following Ref. [2], we take as an approximative solution to Eq. 1 the kink

$$\phi_n\simeq 4\arctan(e^{z_n}). \tag{6}$$

Here $z_n=\sqrt{q}[na-X(t)]$, where $X(t)$ is the slowly varying coordinate of the fluxon center, i.e., X represents the point at which $\phi=\pi$. The parameter q is our continuous version of q_n. If the two values of q_n are uniformly distributed throughout the array, a natural choice is to set $q=\sigma q_A+(1-\sigma)q_B$, where σ is the fraction of occurrences of q_A in the array. Since this is true for the arrays studied here, we will use this approach. The ansatz (6) leads to the following relations for the terms in the energy expression (5):

$$\dot{\phi}_n=-2\sqrt{q}\dot{X}\,\mathrm{sech}(z_n), \tag{7}$$

$$\phi_{n+1}-\phi_n=4\arctan\left[\sinh\left(\frac{a\sqrt{q}}{2}\right)\mathrm{sech}\left(z_n+\frac{a\sqrt{q}}{2}\right)\right], \tag{8}$$

$$1-\cos\phi_n=2\,\mathrm{sech}^2(z_n), \tag{9}$$

$$F\phi_n=4F\arctan(e^{z_n}). \tag{10}$$

Of course, these relations hold only as long as Eq. (6) is a relevant description of the fluxon. This is, however, the case for all situations occurring in this study. In our model the parameters a and q will have values such that $a\sqrt{q}/2\ll 1$ and we can make the approximation $\phi_{n+1}-\phi_n\approx 2a\sqrt{q}\,\mathrm{sech}(z_n)$. We can now write the energy for the Josephson junction array as

$$E = \frac{\dot{X}^2}{2}\underbrace{\sum_n 4q\,\mathrm{sech}^2(z_n)}_{M(X)} + \underbrace{\sum_n 2(q+q_n)\,\mathrm{sech}^2(z_n)}_{U_{\mathrm{sG}}(X)} + \underbrace{\sum_n 4F\arctan(e^{z_n})}_{U_{\mathrm{bias}}(X)}. \tag{11}$$

The effects in the energy resulting from the underlying sequence are collected in the term $U_{\mathrm{sG}}(X)$, whereas $U_{\mathrm{bias}}(X)$ contains the influence of the bias current injected in the junctions. To obtain the effective potential for the single fluxon propagating in the array, we use the fact that the energy is conserved. We start with a fluxon at position $X_0 = an_0$, where n_0 is an integer, and with velocity $\dot{X} = u$. By doing this, we have for the energy $E = u^2 M(X_0)/2 + U_{\mathrm{sG}}(X_0) + U_{\mathrm{bias}}(X_0)$. If we plug this into Eq. 11, we can write this equation as

$$\frac{\dot{X}^2}{2} - \frac{u^2}{2}\frac{M(X_0)}{M(X)} + \frac{[U_{\mathrm{sG}}(X) - U_{\mathrm{sG}}(X_0)]}{M(X)} + \frac{[U_{\mathrm{bias}}(X) - U_{\mathrm{bias}}(X_0)]}{M(X)} = 0. \tag{12}$$

The second term in Eq. 12 is neglected here because $|M(X) - M(X_0)|/M(X) < 10^{-9}$ (at least) and hence it corresponds effectively to a constant downward shift of the potential. If we define the sum of the third and fourth terms to be the effective potential $W(X, X_0)$, the equation reads

$$\frac{\dot{X}^2}{2} + W(X, X_0) = 0. \tag{13}$$

Equation 13 can be thought of as an equation of motion for the fluxon center in the effective potential. $W(X, X_0)$ tells us how a fluxon, with the center originally at X_0, experiences the effective potential at a position X in the array. If we set $z_n^{(0)} = \sqrt{q}(na - X_0)$ and use Eq. 11, the effective potential is given by

$$W(X, X_0) = \underbrace{\frac{\sum_n (q+q_n)[\mathrm{sech}^2(z_n) - \mathrm{sech}^2(z_n^{(0)})]}{2q\sum_n \mathrm{sech}^2(z_n)}}_{W_{\mathrm{sG}}} + \underbrace{\frac{\sum_n F[\arctan(e^{z_n}) - \arctan(e^{z_n^{(0)}})]}{q\sum_n \mathrm{sech}^2(z_n)}}_{W_{\mathrm{bias}}}. \tag{14}$$

This effective potential was, in all essential parts, already obtained in Ref. [9] by the same procedures employed here. We will integrate Eq. 1 numerically and use the effective potential to describe the fluxon motion in a qualitative and sometimes in a quantitative way. The potential will depend heavily on the structure of the underlying sequence. This can be seen in Fig. 1 where the potentials for a periodic (unit cell $q_A q_B$) array and a random array (q_A and q_B are randomly distributed in the same proportions) are shown. Notice the vast difference between these two potentials; this periodic array has an effective potential which approximately is a straight line (dotted line) whereas the random array has an effective potential with local maxima and minima (solid line). How the structure of the potential affects the fluxon motion will be thoroughly examined in Sec. IV.

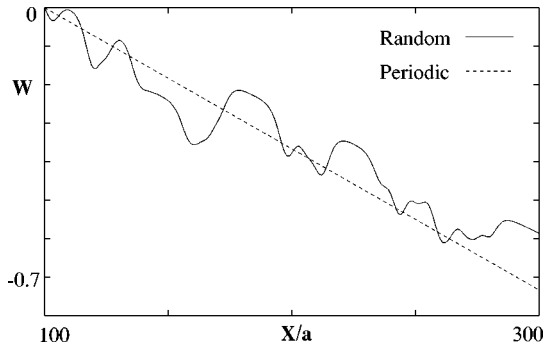

FIG. 1. Effective potential for a periodic (unit cell $q_A q_B$) array (dotted line) and a random array (solid line). The potential for the random array has local maxima and minima but the potential for this periodic array is approximately a straight line. The fluxon will behave differently in these arrays.

IV. RESULTS

The behavior of the fluxon will depend primarily on the array used and the applied bias current. In Fig. 2 we show how the fluxon propagates in a period-doubling array. We note that the kink shape of the fluxon remains approximately the same throughout the propagation. This is a property shared among all the arrays, which means that we can describe the fluxon motion by monitoring the fluxon center, the coordinate X. To further illustrate that the fluxon has soliton properties, we start the fluxon at $n_0 = 180$ in a periodic (unit cell $q_A q_B$) array with $N = 256$. The fluxon will surely hit the boundary, and in Fig. 3 the result of this collision can be seen. The bias drives the fluxon to the right until the fluxon hits the boundary, where it bounces back. This is repeated and we can clearly see the effect of the dissipation as the bounces get shorter and shorter. In the inset in Fig. 3 we also show the corresponding motion of the fluxon center. From

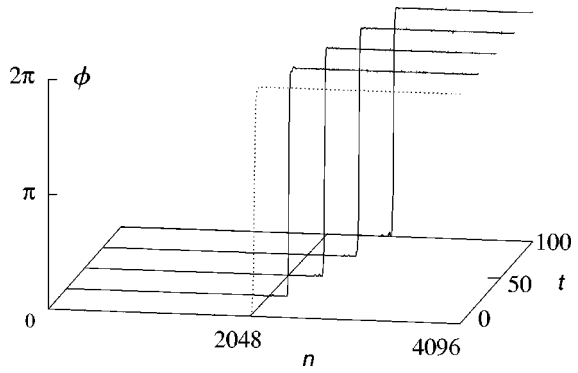

FIG. 2. Propagation of a single fluxon in a period-doubling array. $F=0.11$, $q_B=10$, $N=4096$, and $n_0=2048$. The dotted line is the initial condition for the fluxon and the solid lines are snapshots of the whole fluxon at $t=25$, 50, 75, and 100. The fluxon travels 340 sites with almost constant shape through the array during this time.

these pictures it is evident that the motion of the fluxon can be represented by the motion of its center.

We use the effective potential (14) to predict and describe the dynamics of the fluxon center. The effective potential consists of two parts. The effect of the structure of the underlying sequence on the potential is contained in the term W_{sG} through q_n, and the effect of the applied bias current is reflected in the second term W_{bias} through F. The values of the bias term can be placed on a straight line with a negative slope whenever X/a is an integer. This can be seen in Fig. 4, where W_{bias} is given for different values of F. If X/a is a noninteger, W_{bias} may deviate from a straight line, but for the values used in this study the deviation is bounded by 10^{-3} and therefore neglected. The absolute value of the slope increases linearly with the applied bias (i.e., the potential gets steeper) and is inversely proportional to the square root of q. The former is obvious and the latter can be shown for an infinite array when a is small, and is confirmed for the sequences used here in the inserted diagram in Fig. 4. The part W_{sG} varies between different arrays. For an array where the value of q_n is the same for all junctions, which we will denote as a *monoarray*, W_{sG} is equal to zero if X/a is an integer and otherwise bounded as for W_{bias} (these fluctuations are due to the Peierls-Nabarro potential [14]). A random array has a random distribution of local maxima and minima. We are mainly concerned with deterministic aperiodic arrays. The reason for this is that they have potentials with local maxima and minima just like the random arrays, but unlike the random arrays they are completely known so that it is easier to make predictions for the motion of the fluxon. Some of the deterministic aperiodic sequences have a special self-similarity which is reflected in the potentials. This can be seen in Fig. 5, where W_{sG} is shown for a Fibonacci array and a period-doubling array. The effective potential is the sum of the above-mentioned parts, where the effect of the bias current is to press down the potential and drive the fluxon to the right. An example of how the applied bias current affects the potential can be seen in Fig. 6, where a part of the effective potential for a period-doubling array consisting of 500 junctions is shown for various values of the bias current. Domínguez-Adame *et al.* [9] have shown that the fluxon can be pinned in an aperiodically ordered array under certain conditions. It seems reasonable that the fluxon can be pinned in the local minima of the effective potential. For large values of F the potential is almost a straight line but for low values the local maxima and minima are more pronounced. This implies that there should exist a certain critical bias current F_c, such that for $F>F_c$ the fluxon will start to propagate freely in the array and for $F\leqslant F_c$ the fluxon will get pinned. This is indeed the case and the critical bias current depends on the parameters of the junction array, e.g., the ordering of the array, the values of the material parameters, the distance between the junctions, and the starting site for the fluxon.

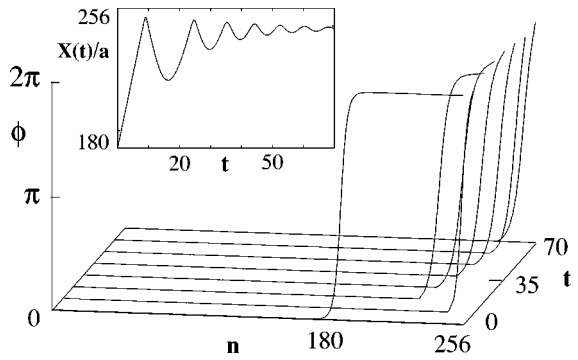

FIG. 3. Soliton properties of the fluxon in a periodic (unit cell q_Aq_B) array consisting of 256 junctions, where $q_B=10$. The fluxon collides with the boundary but retains its shape. Inset: The corresponding motion of the fluxon center. Note the effect of the dissipation as the bounces get shorter and shorter.

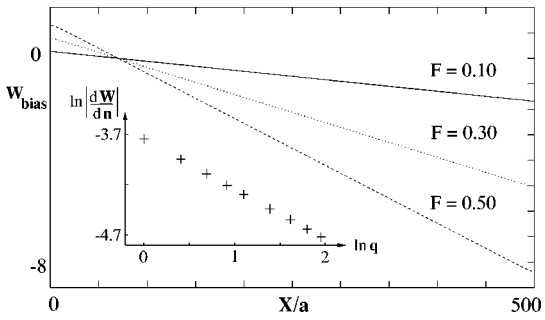

FIG. 4. W_{bias} for $F=0.1$, 0.3, and 0.5. The slope of W_{bias} gets steeper as the bias is increased. The inserted diagram shows that the absolute value of the slope of W_{bias} varies as $1/\sqrt{q}$.

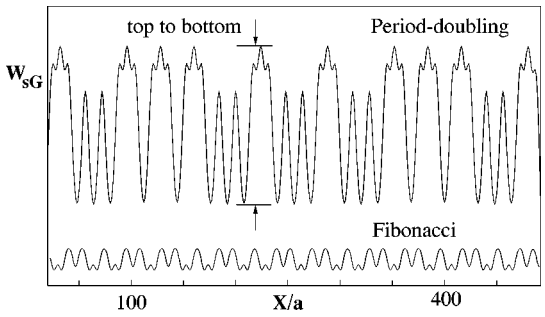

FIG. 5. W_{sG} for a period-doubling array and a Fibonacci array both having $q=4$. The self-similarity of the sequences is reflected in the potentials. The top to bottom value is a measure of variations of the amplitude in W_{sG}. The period-doubling array has in this case a value of 0.113, and the Fibonacci array has a value of 0.015.

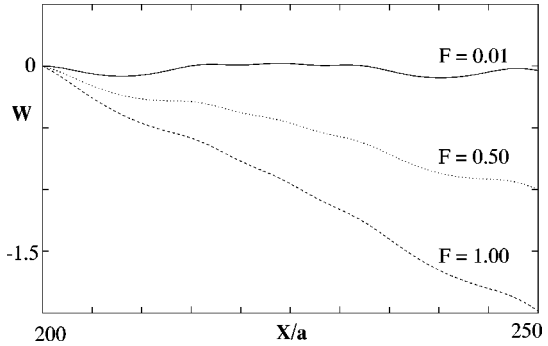

FIG. 6. Effective potential for a period-doubling array for $F=0.01,0.5$, and 1.0. The maxima and minima are suppressed when the bias is increased.

Fluxon pinning

To investigate how the dynamics of the fluxon is connected to the effective potential, we use the period-doubling array as a first example. In Fig. 7(a) the effective potential for $F=0.02$ is shown. Figure 7(b) shows the motion of the fluxon center. We see that it first accelerates down the slope of the effective potential, and when it reaches the minimum the velocity is high enough to let the fluxon start to climb up the potential well. The fluxon slows down and eventually the velocity becomes zero and the fluxon drops back down in the well. This repeats itself a couple of times and leads to an oscillating motion. Due to the dissipation, the fluxon finally comes to rest at site 2064, exactly at the minimum in the effective potential.

When F is increased the fluxon will not get pinned in the same minimum as before. The result from a simulation with $F=0.05$ can be seen in Fig. 7(c). The fluxon velocity at the bottom of the first minimum is high enough to let the fluxon escape from the potential well. We see in the figure that the velocity decreases as the fluxon climbs up the hill. After this, the fluxon accelerates down the second large minimum at site 2096 and climbs up that well also, but in the third large minimum at around site 2112 the fluxon gets pinned. Because we have neglected the dissipative term and $t\gg 0$, we can only see what are the possible pinning positions from the potential, but not where the fluxon actually will be pinned. Figure 7(d) shows the case with $F=0.12$ where the situation is about the same, but now $F>F_c$ for this array so that the fluxon has enough velocity to overtake all minima and starts to propagate in the array. There are still small changes in the velocity due to the different maxima and minima in the potential but as F increases these will be less prominent.

Let us return to the effective potential for this array. To further confirm its connection with the fluxon dynamics, we have performed a simulation where we choose $n_0=2064$ as the initial site. This site corresponds to the first large minimum in the effective potential in Fig. 7(a). The bias current is $F=0.05$, a value for which the fluxon did not get pinned when it started from the initial site $n_0=2048$. Now the situation is different and, as can be seen in Fig. 8, the fluxon gets pinned. Initially the fluxon is in a potential minimum and the bias current drives the fluxon to the right. Unlike before, the velocity is now not large enough to bring the fluxon out of the potential well and it is pinned. This also exemplifies that the starting position of the fluxon influences the critical bias current F_c.

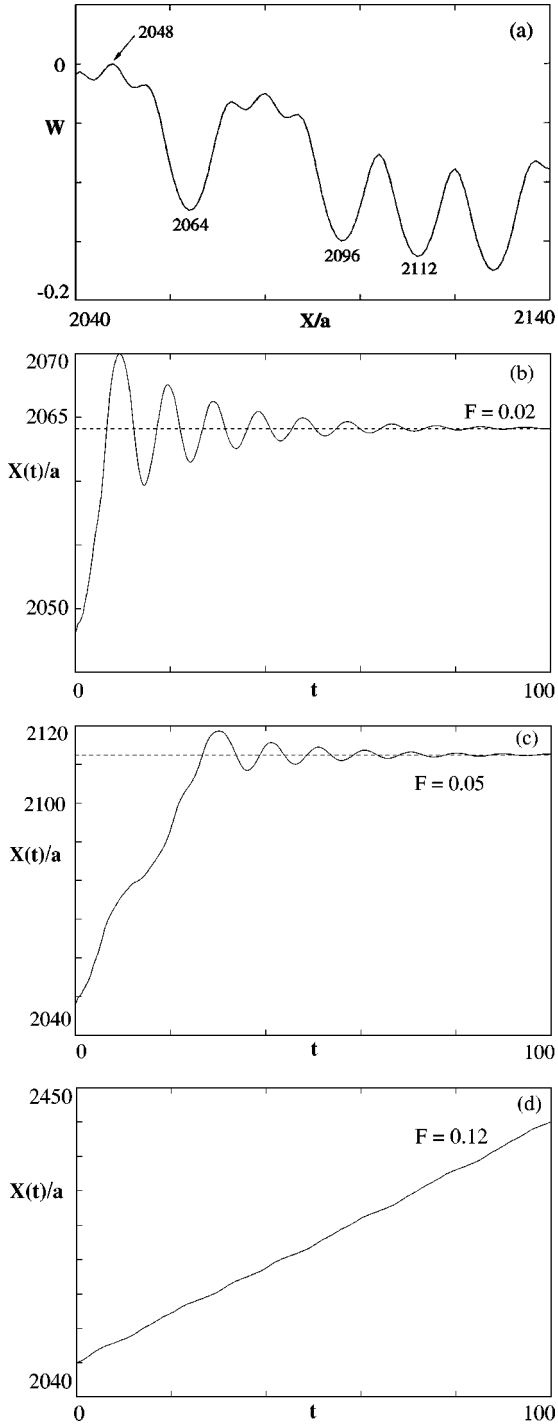

FIG. 7. Fluxon in a period-doubling array. $N=4096$, $n_0=2048$, and $q_B=10$. (a) Effective potential for $F=0.02$. (b) Pinning of the fluxon center at site 2064 corresponding to the first large minimum in the effective potential. (c) Pinning of the fluxon center at 2112. (d) $F>F_c$ for this array which implies that the fluxon propagates freely. [The effective potentials for the bias currents used in (c) and (d) have the same structure as that in (a) but are tilted downwards due to the higher values of the bias currents.]

The minima in the effective potential of the period-doubling sequence are smooth and symmetric, leading to the well-behaved motion of the fluxon center in, e.g., Fig. 7(b).

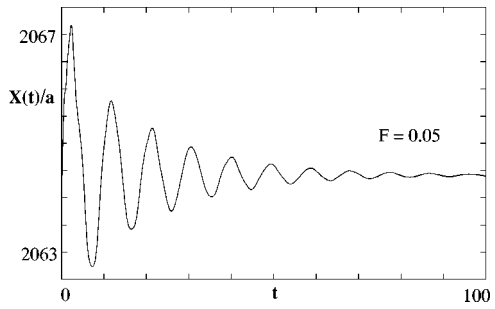

FIG. 8. Pinning of the fluxon center at approximately site 2064. Same parameters as in Fig. 7 except that $n_0=2064$, i.e., the first large minimum in the potential in Fig. 7(a). The fluxon did not get pinned at this site for $F=0.05$ when it started at $n_0=2048$.

The situation is different for the paper-folding array, which can be seen in Fig. 9(a). The minimum at site 2083 is asymmetric and not as steep to the right as to the left. If the fluxon gets pinned in this minimum, it can deviate more from the equilibrium to the right-hand side. In Fig. 9(b) we see a fluxon being pinned in the minimum at site 2083 and we clearly see that the fluxon moves further up the potential well to the right side as predicted from the effective potential.

Fluxon propagation

When the applied bias exceeds F_c, the fluxon will propagate through the array. For a monoarray $F_c=0$ and the fluxon propagates for $F>0$ (the discreteness parameter a is chosen such that the Peierls-Nabarro potential is negligible).

In Ref. [9] the following formula is proposed for calculating the final velocity u_∞ for a fluxon:

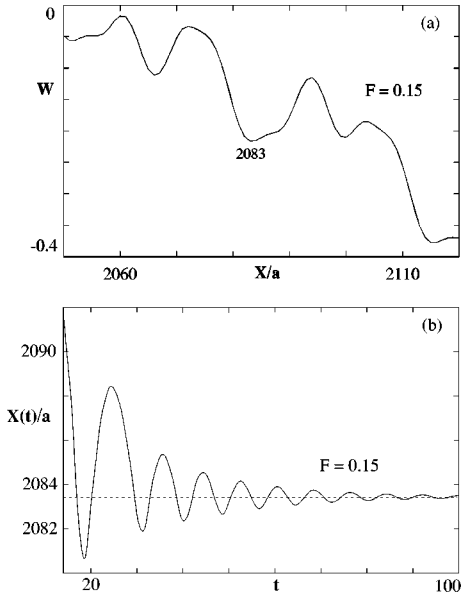

FIG. 9. Pinning of the fluxon center in a paper-folding array. Same parameters as in Fig. 7. (a) Effective potential for $F=0.15$ around site 2083, where the potential minimum is asymmetric. (b) Motion of the fluxon center as the fluxon gets pinned in the minimum at site 2083. The fluxon deviates more from the equilibrium position to the right because the potential is less steep in that direction.

TABLE II. Comparison between the final velocity of the fluxon in different arrays. According to Eq. 15 the velocities are $u_\infty=0.762$ ($F=0.3$) and $u_\infty=0.891$ ($F=0.5$). The top to bottom values (see Fig. 5 for definition) are the relative heights compared to the Fibonacci array value, which is set to 1.

Array	$F=0.3$	$F=0.5$	Top to bottom
Monoarray	0.761	0.881	0.0
Fibonacci	0.760	0.880	1.0
Thue-Morse	0.756	0.880	1.4
Period-doubling	0.745	0.877	7.5
Paper-folding	0.735	0.877	9.3
Rudin-Shapiro	0.695	0.872	24.4

$$u_\infty=\left[1+q\left(\frac{4\alpha}{\pi F}\right)^2\right]^{-1/2}. \tag{15}$$

This equation, however, is derived from the continuous sine-Gordon equation, which means that it is not necessarily applicable to discrete systems. Nevertheless, Eq. 15 gives reasonable values (within 1%) when $0.1\leqslant F\leqslant 0.3$ (and $F>F_c$) for the predicted velocities for monoarrays, the Fibonacci array, and the Thue-Morse array. For other arrays, especially those which have irregular effective potentials, the agreement is not that good. Also, the agreement is not that good for higher values of the bias current.

We measure the final velocities for the fluxon in the deterministic aperiodic arrays and a monoarray, all of which have $q=4.0$. In these cases, the velocity might vary as a function of position of the fluxon in the array, due to irregularities in the effective potentials. We then estimate the mean velocity after some time when all the transient properties, such as dependence of initial site, are lost. We use two different values for the bias, $F=0.3$ and $F=0.5$, which by use of Eq. 15 gives the velocities $u_\infty=0.762$ and $u_\infty=0.891$, respectively. The results are summarized in Table II. For $F=0.5$, Eq. 15 does not yield a good agreement even for a monoarray. The velocities are lower than expected, which was already noted in Ref. [15]. We attribute this discrepancy to the fact that if the bias is large, so is the fluxon velocity, leading to a more narrow kink. This yields more prominent discreteness effects which spoil the continuum approximation (for $a<0.1$ the agreement gets better, and for $a>0.1$ the deviation increases). Neither does the proposed formula take into account the ordering of the arrays. We have seen that the effective potentials differ in structure, but their relative magnitudes are also different. A measure of the variations is the top to bottom value, which is defined in Fig. 5. An example of this is given in Fig. 10, where W_{sG} is given for a Thue-Morse array and a Rudin-Shapiro array. The potential for the Rudin-Shapiro array contains more drastic variations, which means that the fluxon meets more resistance when propagating. The Fibonacci array has the smallest top to bottom value for the potential among the aperiodic arrays and the highest fluxon velocity. The Thue-Morse array has a top to bottom value which is 1.4 times larger than the Fibonacci array and a slightly lower velocity. The corresponding relations for the other arrays are period-doubling 7.5, paper-folding 9.3, and Rudin-Shapiro 24.4 relative to the Fibonacci array. This or-

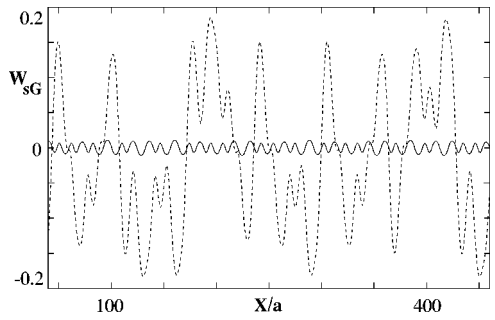

FIG. 10. W_{sG} for a Thue-Morse array (solid line) and Rudin-Shapiro array (dashed line) both having $q=4$. The Rudin-Shapiro array has larger variations in the potential than the Thue-Morse array, which restrains the fluxon propagation more.

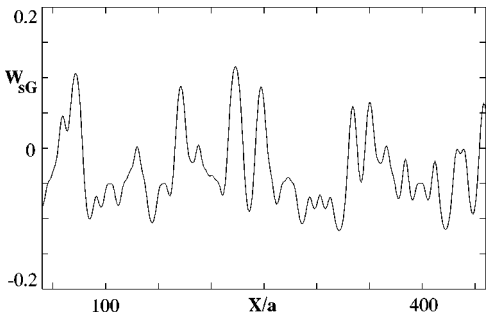

FIG. 11. W_{sG} for a period-doubling-like sequence generated through a fourth-order Markov process. Compare Fig. 5, in which the parameter values are the same.

dering is the same as for the velocities from Table II. Although the effective potential does not incorporate the dissipative effects in the system and hence its applicability for describing the propagating fluxons is limited, this ordering supports the statement that the velocity is lowered for arrays with potentials which contain large fluctuations.

The fluxons from different arrays have a small spread in their velocities at higher values of the bias current. This can be explained if we examine Fig. 4. When the bias is increased, the effective potential is tilted downwards so that the local maxima and minima are suppressed and the potential decreases monotonically. This behavior is universal to all the arrays and allows the fluxon to propagate with approximately the same speed in all cases, for large enough bias.

Effects of long-range order

We want to see what happens to the fluxon motion if a sequence only has local order. To accomplish this we make period-doubling-like arrays through Markov processes of different orders in the same way as in, e.g., Ref. [16]. For example, when we simulate the period-doubling sequence with a three-state Markov process, we start with the first two elements being AB (as in the real period-doubling sequence) and then use the conditional probabilities $P(A|AB)$ and $P(B|AB)$ from Ref. [17], and a random number generator to obtain what should be the third element of the sequence. In the same way, we obtain the fourth element by considering the second and third elements and the conditional probabilities based upon our knowledge of these elements. By continuing this process we get a random sequence which has the same short-range order as the period-doubling sequence, but without any long-range order. Generally, in a sequence generated by an nth-order Markov process, the conditional probability to obtain a specific element is based on the knowledge of the $(n-1)$ previous elements. This means we have to start with a knowledge of the $n-1$ first elements of the sequence we mimic. This was also done in Ref. [18] for the Fibonacci chain with a three-state Markov process. There it was numerically shown that the quasiperiodic diffraction pattern, which is crucially dependent on the long-range order, ceases to exist and instead one gets a continuous distribution, just as in the case of an amorphous material.

Figure 11 shows W_{sG} for a sequence generated by a fourth-order process, having the same parameter values as the period-doubling sequence in Fig. 5. For this realization the potential does not bear much resemblance to that of the period-doubling array, except for a small part at site 300. Different Markov generated sequences give rise to different behavior for the fluxon motion at low bias currents, e.g., different pinning sites. For higher biases the fluxon propagates with the same constant velocity as could be expected from the discussion above. The conclusion is that the order of the junctions is of little effect for the fluxon propagating in the array, but not the proportions of each type of junction. The ordering of the junctions becomes important when the detailed dynamics of the fluxon is to be considered, e.g., small variations in the velocity at bias currents just above F_c or the pinning of the fluxon. The self-similarity that the substitution sequences possess, and that the Markov-generated sequences lack, is reflected in the shape of the effective potential, being in some sense regular in the former case, but not in the latter.

These results are in accordance with Ref. [9], where another approach is used to study the effects of long-range order. There, different periodic approximants of the Fibonacci sequence are used for a study of how the critical bias current F_c and the final velocity of the fluxon varies with the length of the periodicity of the sequence. The final velocity turns out to agree with the result from an array ordered according to the Fibonacci sequence when the length of the unit cell exceeds the extension of the fluxon. Otherwise, the velocity is slightly reduced. This is in correspondence with our finding that the effects of long-range order are of little importance for the propagation of the fluxon. The value of the critical bias current increases with the length of the unit cell, and no saturation is found (up to a unit cell consisting of 144 elements). This is a case of detailed dynamics, and accordingly the ordering should be important, just as it turns out.

A shift register

We finish with a study of how the array can be arranged so that the minima of the potential are distributed in a way that appeals to us. The dotted line in Fig. 12 shows W_{sG} for a periodic array with a unit cell consisting of 20 junctions, the first 16 having the value $q_A=1$ and the last four $q_B=6$. For this array, with evenly spaced minima in the potential, a simulation is performed where the dissipative constant $\alpha=0.2$ and the bias current is injected in the form of a repeated square pulse wave of period $T=25$ with a duration of $\Delta T=0.5$,

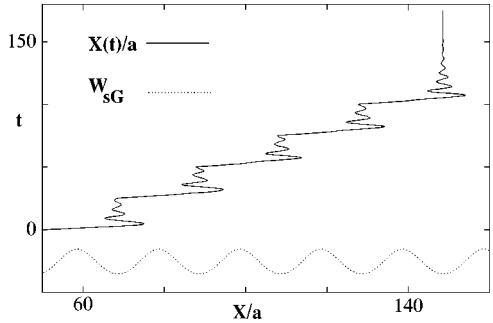

FIG. 12. Fluxon in periodic (unit cell $16q_A4q_B$) array. $N=256$, $n_0=50$, $q_B=10$, and $\alpha=0.2$. The dotted line shows the W_{sG} part of the potential, which has evenly spaced minima. The bias current is injected in the form of a square pulse wave which forces the fluxon to make a transition from the minimum it is situated in to the next, where it gets pinned again.

$$F(t)=\begin{cases}3.0, & \text{if} \quad mT<t<mT+\Delta T, \quad m=0,1,2,3,4\\ 0.0 & \text{otherwise.}\end{cases} \tag{16}$$

The solid line in Fig. 12 displays the position of the fluxon center for times $0<t<175$. When the bias current is turned on, the fluxon shifts to the next potential minimum where it gets pinned until the next current injection. This could, e.g., be used as a shift register. One might guess that a bias injection in the form of Eq. 16 would have the same effect on a monoarray. That this is not true can be seen from Fig. 13, where this case applies. The fluxon is not pinned immediately after the bias is turned off. Instead the velocity of the fluxon decreases monotonically and the position where the fluxon stops depends more crucially on the parameter values used. The spatial localization of the fluxon center obtained in the first case is thereby lost.

V. SUMMARY

We have studied different aspects of fluxon motion in one-dimensional arrays of Josephson junctions when the order of the junctions has been aperiodic. The dynamics of the fluxon is governed by the discrete sine-Gordon equation, where we have inserted two extra terms, corresponding to dissipation and a bias current, respectively. Our principal tool in the investigation has been an effective potential, which consists of one part reflecting the order of the array and the other part the influence of the bias current. It is shown by some examples of direct integration of the equations of motion that the effective potential is rather well-suited for describing the dynamics of the fluxon, although it does not incorporate the dissipative effects, which limits its usefulness somewhat.

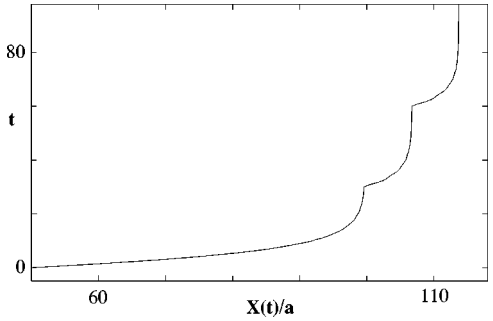

FIG. 13. Motion of the fluxon center in a monoarray, where $q=4.0$. The bias current is in the form of the same square pulse wave as in Fig. 12 (except $T=30$). When the bias is turned off, the fluxon does not stop immediately, but the velocity decreases gradually.

The effective potential shows very different behavior dependent upon which ordering we consider. In a monoarray, it is approximately a straight line, which means that the fluxon can propagate freely in the array. For the aperiodic arrays the potential contains local maxima and minima of various amplitudes, and it is shown that the fluxon can get pinned in a local minimum. From the effective potential we get the possible pinning positions in the array, although not which one it will actually be in a specific case. The effect of the bias current is mainly to be an energy injection which drives the fluxon in a specific direction. This can be seen from the potential where a higher value of the current results in a larger slope of the potential. The velocity of a propagating fluxon is a function of the bias current, the dissipation, and the mean value of the material parameters, but also of the variation in amplitude of the effective potential and the discreteness of the array.

Finally, we have shown one example of how the potential can be used to customize an array to have exactly the properties we like. In this case we used a periodic array to construct a device which effectively is nothing but a shift register.

ACKNOWLEDGMENTS

We would like to thank Magnus Johansson, Bruno Lindquist, and Rolf Riklund for valuable comments and criticism, which have improved the readability of the paper considerably. Partial financial support from the Swedish Natural Science Research Council is gratefully acknowledged.

[1] S. Watanabe, H. S. J. van der Zant, S. H. Strogatz, and T. P. Orlando, Physica D **97**, 429 (1996).
[2] M. Salerno and Yu. S. Kivshar, Phys. Lett. A **193**, 263 (1994).
[3] J. Frenkel and T. Kontorova, J. Phys. (Moscow) **1**, 137 (1939).
[4] A. Barone and G. Paternó, *Physics and Applications of the Josephson Effect* (Wiley, New York, 1982).
[5] A. Janner, T. Janssen, and P. M. de Wolff, Europhys. News **13**, 1 (1982), and references therein.
[6] D. Shechtman, I. Blech, D. Gratias, and J. W. Cahn, Phys. Rev. Lett. **53**, 1951 (1984).
[7] R. Merlin K. Bajema, R. Clarke, F.-Y. Juang, and P. K. Bhattacharya, Phys. Rev. Lett. **55**, 1768 (1985).

[8] M. Hörnquist and T. Ouchterlony, Physica E **3**, 213 (1998); W. Ping, W. Feng, and X. Wu, J. Infrared Millim. Waves **11**, 145 (1992).
[9] F. Domínguez-Adame, A. Sánchez, and Yu. S. Kivshar, Phys. Rev. E **52**, 2183 (1995).
[10] H. S. J. van der Zant, M. Barahona, A. E. Duwel, E. Trías, T. P. Orlando, S. Watanabe, and S. Strogatz, Physica D **119**, 219 (1998).
[11] M. Hörnquist, J. Phys. A **30**, 7057 (1997), and references therein.
[12] M. Mendès France and A. J. van der Poorten, Bull. Austral. Math. Soc. **24**, 123 (1981).
[13] D. W. McLaughlin and A. C. Scott, Phys. Rev. A **18**, 1652 (1978).
[14] M. Peyrard and M. D. Kruskal, Physica D **14**, 88 (1984).
[15] J. F. Currie, S. E. Trullinger, A. R. Bishop, and J. A. Krumhansl, Phys. Rev. B **15**, 5567 (1977).
[16] M. Hörnquist and R. Riklund, J. Phys. Soc. Jpn. **65**, 2872 (1996).
[17] K. W. Sulston, B. L. Burrows, and A. N. Chishti, Physica A **217**, 146 (1995).
[18] M. R. Schroeder, *Number Theory in Science and Communication*, 3rd ed., Springer Series in Information Sciences (Springer-Verlag, Berlin, 1997).